UCLA
UCLA Previously Published Works

Title

Crystal structure of arginine-bound lysosomal transporter SLC38A9 in the cytosol-open state

Permalink

Journal

ISSN

Authors

Lei, Hsiang-Ting
Ma, Jinming
Sanchez Martinez, Silvia
et al.

Publication Date

DOI

Peer reviewed

Crystal structure of arginine-bound lysosomal transporter SLC38A9 in the cytosol-open state

Hsiang-Ting Lei [1,4], Jinming Ma[1,2,4], Silvia Sanchez Martinez [1] and Tamir Gonen [1,2,3]*

Recent advances in understanding intracellular amino acid transport and mechanistic target of rapamycin complex 1 (mTORC1) signaling shed light on solute carrier 38, family A member 9 (SLC38A9), a lysosomal transporter responsible for the binding and translocation of several essential amino acids. Here we present the first crystal structure of SLC38A9 from *Danio rerio* in complex with arginine. As captured in the cytosol-open state, the bound arginine was locked in a transitional state stabilized by transmembrane helix 1 (TM1) of drSLC38A9, which was anchored at the groove between TM5 and TM7. These anchoring interactions were mediated by the highly conserved WNTMM motif in TM1, and mutations in this motif abolished arginine transport by drSLC38A9. The underlying mechanism of substrate binding is critical for sensitizing the mTORC1 signaling pathway to amino acids and for maintenance of lysosomal amino acid homeostasis. This study offers a first glimpse into a prototypical model for SLC38 transporters.

SLC38A9 is a member of the SLC38 class of sodium-coupled transporters[1,2]. Classified within the amino acid–polyamine organocation (APC) superfamily[3], SLC38A9 belongs to the amino acid/auxin permease (AAAP) subfamily[4]. Thus far, members of the AAAP family have been found only in eukaryotic systems and share features like an extended N-terminal soluble domain and 11 transmembrane helices[4,5]. In humans, at least 17 AAAP members have been found[6], spanning the SLC32, SLC36 and SLC38 solute carrier families, although no structures have been determined so far. Transporters in the SLC32, SLC36 and SLC38 families essentially comprise half of the mammalian amino acid transport systems, with the other half consisting of SLC7 and SLC12 family members[7]. Regardless of the key roles of these transporters in mammalian physiology, there are few studies on the molecular principles underlying substrate binding, sodium ion selectivity and the transport mechanism. To obtain a structural basis for the AAAP family that would allow exploration of mechanistic insights, we set out to solve the structure of a vertebrate homolog of human SLC38A9. Notably, besides its ability to transport a variety of amino acids across the lysosomal membrane, SLC38A9 is also known to participate in the Ragulator–Rag GTPase complex and has an important role in the amino acid–dependent activation of mTORC1[1,2]. As such, SLC38A9 can be thought of as a 'transceptor', as it embodies two distinct and complementary functions: one as a transporter and the other as a receptor.

The first member of the SLC38 family was cloned in 2000[8,9], namely sodium-coupled neutral amino acid transporter 1 (SNAT1), encoded by the *slc38a1* gene. Currently, 6 of the 11 SLC38 proteins have been characterized and integrated into two functional types named system A and system N[10]. SNAT1, SNAT2 and SNAT4 have a hallmark of transport activity inhibition by methylaminoisobutyrate (MeAIB), an amino acid analog, and are hence referred to as system A. SNAT3, SNAT5 and SNAT7 are resistant to MeAIB and are referred to as system N[11]. SLC38A9 (SNAT9) is also resistant to MeAIB and is therefore a member of system N[1]. However, the broad substrate specificity of SLC38A9 is reminiscent of those of system A

transporters[12]. The increasing ambiguity between system A and system N transporters necessitates deep analyses of substrate binding and transport among the SLC38 family members. Here we present the crystal structure of SLC38A9 from zebrafish to demonstrate the binding mechanism for L-arginine in the transport cycle.

Results

Overall architecture and the luminal gating network of arginine-bound drSLC38A9. In the present study, we determined the crystal structure of SLC38A9 from zebrafish (*Danio rerio*; drSLC38A9 hereafter) in complex with arginine at 3.17Å resolution (Fig. 1a,b and Table 1). This transporter consists of 11 transmembrane helices, with its N terminus located in the cytosol and its C terminus on the luminal side of the membrane (Fig. 1a). Consistent with other members of the APC superfamily[6], drSLC38A9 adopts a LeuT-like pseudosymmetric bundle of five transmembrane helices forming an inverted-topology repeat: the N-terminal half consists of TM1–TM5, and the C-terminal half consists of TM6–TM10. TM11 flanks the transporter on one side. TM1 and TM6 are broken and line the substrate-binding site, where an arginine molecule was identified (Fig. 1b). Sequence alignment of this protein from zebrafish, frog, mouse and human indicates that the 11 transmembrane regions are highly conserved (Supplementary Note 1). drSLC38A9 has 61.9% identity and 86.6% similarity with the human homolog (hSLC38A9) (Supplementary Note 1). Despite major efforts to crystallize full-length drSLC38A9, only an N-terminally truncated form (ΔN-drSLC38A9) yielded ordered crystals amenable to diffraction studies. An antibody fragment, Fab-11D3, was used to further stabilize the luminal loops and optimize crystallization (Supplementary Figs. 1 and 2). As shown by an arginine uptake assay using drSLC38A9-reconstituted liposomes (Fig. 1c), the truncated drSLC38A9 protein is active and able to bind arginine similarly to the wild-type protein.

SLC38A9 is a member of the sodium-coupled amino acid transporters[1,2]. As is often the case with these proteins, a density corresponding to a sodium ion was not identified in the structure

[1]Janelia Research Campus, Howard Hughes Medical Institute, Ashburn, VA, USA. [2]Howard Hughes Medical Institute, University of California, Los Angeles, Los Angeles, CA, USA. [3]Departments of Physiology and Biological Chemistry, David Geffen School of Medicine, University of California, Los Angeles, Los Angeles, CA, USA. [4]These authors contributed equally: Hsiang-Ting Lei, Jinming Ma. *e-mail: tgonen@ucla.edu
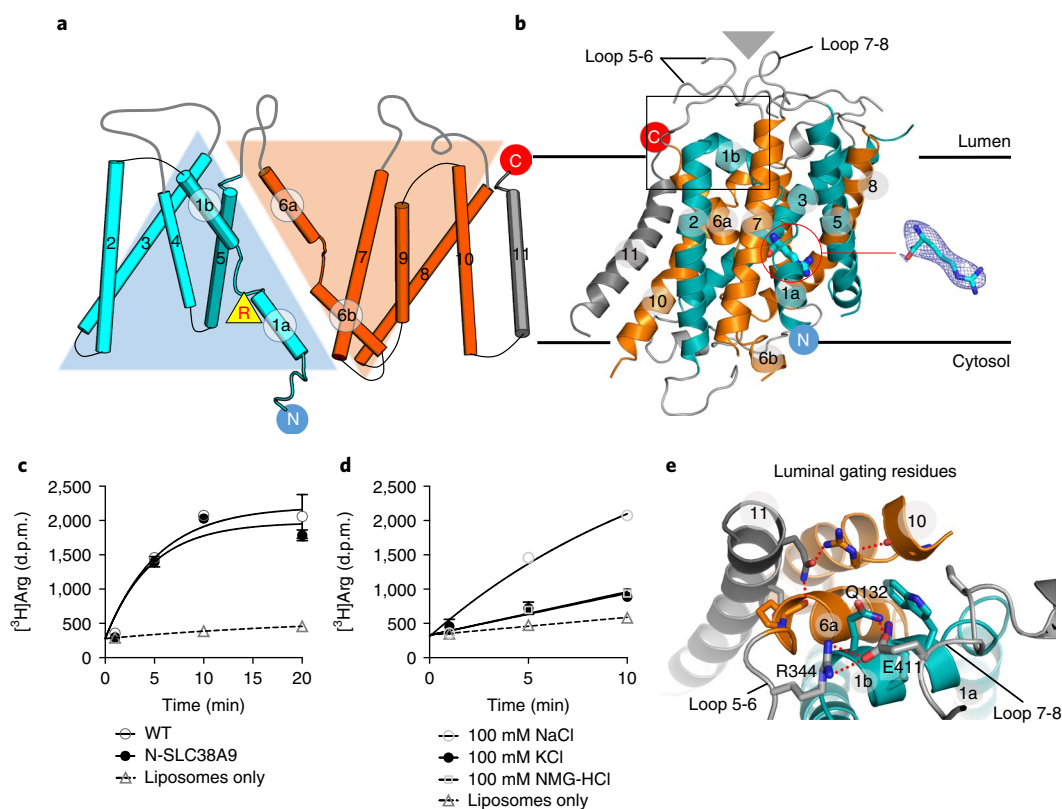
Fig. 1 | Overall architecture and the luminal gating network of arginine-bound drSLC38A9. a, 2D topology model of drSLC38A9. The first ten transmembrane helices are folded into a characteristic twofold LeuT-like pseudosymmetry (five transmembrane helices in an inverted-topology repeat). Bound arginine is marked by a filled yellow triangle, next to the TM1a helix. Cyan, TM1–TM5; orange, TM6–TM10; gray, TM11. **b,** drSLC38A9 structure on the lysosomal membrane. Transmembrane helices are colored as in **a**. The position of the Fab fragment is shown by a gray triangle above the luminal loops. Lumen and cytosol domains are equivalent to extracellular (out) and intracellular (in) domains for a transporter expressed on the cell plasma membranes. An arginine (blue stick) is identified at the binding site next to TM1a. A 2mFo-DFc map contoured at 1.0σ is shown for the arginine. **c,** Uptake assay in drSLC38A9-reconstituted liposomes showing that the efficiency of arginine transport is similar for the wild-type protein and the truncated drSLC38A9 used for crystallization. Error bars, s.e.m. from three independent proteoliposome preparations; $n = 3$ biological replicates (Supplementary Dataset 1). **d,** Uptake assay of liposomes reconstituted with wild-type drSLC38A9 in buffers containing sodium, potassium or NMG cations, showing the sodium-dependent transport of arginine. The presence of sodium significantly increased the uptake of L-arginine, as compared to potassium (unpaired t test, $P = 0.0007$) and NMG (unpaired t test, $P = 0.0005$). Error bars, s.e.m. from three independent proteoliposome preparations; $n = 3$ biological replicates (Supplementary Dataset 1). **e,** Enlarged view of the boxed region in **b** encompassing the luminal gating residues. Glu411 of loop 7-8 acts as a network hub in the luminal gating of drSLC38A9, joined by Lys131 and Gln132 of TM1b and Arg344 of loop 5-6.

presented here. Instead, functional assays were performed to shed light on the possible coupling mechanism. Uptake assays with drSLC38A9-reconstituted liposomes were performed in buffers containing sodium, potassium or N-methyl-D-glucamine (NMG) (Fig. 1d). While uptake of arginine in the presence of potassium or NMG was not observed, robust uptake was observed in the presence of sodium. These results indicate that sodium is required for arginine uptake by SLC38A9, although it is not clear whether the sodium only binds to (and thereby activates) the transporter or if the sodium ion is also co-transported with the amino acid.

Because SLC38A9 is found in the lysosomal membrane, its cytosol-open state resembles an inward-open state for a transporter found in the cell plasma membrane (Fig. 1b). Superposition of drSLC38A9 on the arginine–agmatine antiporter AdiC[13] indicates that drSLC38A9 in the cytosol-open state may undergo major conformational changes occurring at TM1 and TM6 during transport (Supplementary Fig. 3). In the cytosol-open state presented here, the luminal gate is closed while the cytosol side consists of a wide vestibule open to the cytoplasm (Figs. 1e and 2). On the luminal side, polar interactions of residues on TM1b, loop 5-6 and loop 7-8 with residues on TM6a, TM10 and TM11 prevent solvent access

to the substrate-binding site toward the center of the transporter (Fig. 1b,e). Unlike other APC transporters (such as LeuT, BetP, CaiT and MhsT) in their inward-open state[14–17], drSLC38A9 does not use an inner gating system in its central region to keep solvent out. In contrast, it closes its luminal surface through the peripheral polar groups of Lys131 and Gln132 on TM1b, Arg344 on loop 5-6 and Glu411 on loop 7-8 (Fig. 1e).

Arginine bound in the cytosol-open conformation of drSLC38A9. drSLC38A9 was crystallized in the presence of its substrate arginine. The electron density map allowed us to identify an arginine molecule bound close to the center of drSLC38A9, adjacent to TM1a (Figs. 1b and 2). Recognition of arginine at this location involves interactions with Thr117, Met119, Thr121 and Ser122 from TM1a, Tyr204 from TM3 and Gln438 from TM8. The α-amino group of arginine is hydrogen bonded to Thr121 and Ser122, and is further stabilized by the 4-hydroxyl group of Tyr204 across the cytoplasmic vestibule on TM3 (Fig. 2a). Notably, a surface area made from the backbone carbonyl groups of Asn116, Thr117, Met118 and Met119 electrostatically draws the guanidinium group of the bound arginine adjacent to TM1a (Fig. 2b). It has been shown in the human

Table 1 | Data collection and refinement statistics

	SLC38A9–11D3 (native)[a] (PDB 6C08)	SLC38A9–11D3 (Se-Met)
Data collection		
Space group	$P12_11$	$P12_11$
Cell dimensions		
a, b, c (Å)	136.61, 82.81, 158.92	136.163, 82.795, 158.922
α, β, γ (°)	90, 100.02, 90	90, 100.005, 90
Resolution (Å)	3.1	3.358
R_{meas}	0.127 (1.642)	0.07465 (1.812)
$I/\sigma(I)$	8.3 (1.1)	12.71 (0.86)
$CC_{1/2}$	0.997 (0.6)	0.999 (0.347)
Completeness (%)	99.8 (98.1)	96.98 (81.17)
Redundancy	8.3 (8.5)	3.4 (3.2)
Refinement		
Resolution (Å)	156.5 –3.17 (3.283 –3.17)	
No. reflections	58,098 (5,909)	
R_{work} / R_{free}	0.2670/0.2850 (0.3580/0.3721)	
No. atoms		
Protein	12,332	
Ligand/ion	1 arginine	
B factors	113.00	
SLC38A9	141.23	
11D3-Fab	88.75	
Arginine	147.08	
R.m.s. deviations		
Bond lengths (Å)	0.006	
Bond angles (°)	1.36	

[a]Merged from two crystals.

Fig. 2 | Arginine bound in the cytosol-open conformation of drSLC38A9. **a**, View from the carboxylate group of arginine. The TM1a binding site is surrounded by TM1a, TM3, TM6b, TM5 and TM8. The α-amino group of arginine is bonded to the β-hydroxyl groups of Thr121 and Ser122. The carboxylate group of arginine is bonded to Tyr204. **b**, View from the guanidinium group of arginine. The positively charged group is stabilized by Thr117 and Met119 on TM1a and by Gln438 on TM8. **c**, Schematic of the drSLC38A9 and arginine interactions shown in **a** and **b**. Dotted lines depict hydrogen bonds. **d**, Surface presentation of drSLC38A9 in the cytosol-open state. TM1 and TM6 are colored in cyan and orange, respectively.
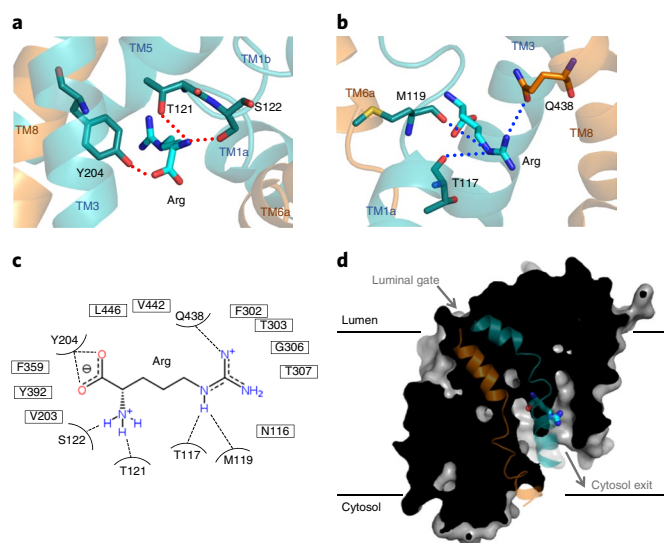
homolog that a Thr133Gln substitution (equivalent to a Thr121Gln substitution in the present structure) abrogates transport activity for arginine[18]. Indeed, in our structure, Thr121 is a key residue involved in stabilizing the bound arginine.

TM1 stabilizes arginine at the TM1a binding site in drSLC38A9. As TM1 and TM6 change conformation, they affect the location and bonding of arginine. The arginine in drSLC38A9 was found at a different location than the arginine in AdiC (Fig. 3a). In AdiC, an arginine molecule was observed at the center of the transporter, lying roughly parallel to the plane of the membrane. However, in drSLC38A9, which is open to the cytosol, the arginine had a different orientation in which it pointed toward the cytosol (Fig. 3a). This orientation of the arginine is stabilized by interactions with TM1a. Binding at the TM1a site requires a specific geometry of the amino acid, such as an elongated, positively charged side group. The location of the bound arginine in drSLC38A9 is distinct from that of other substrates found in transporters that were also captured in an inward-open or occluded conformation, for example vSGLT, BetP, CaiT and MhsT[15–17,19]. For drSLC38A9, the unique binding site of arginine suggests that the present structure could represent a divergent intermediate state in the transport cycle that arises upon arginine binding (Fig. 3b).

The asymmetric unit in our crystals contained two molecules of drSLC38A9, one with bound arginine and the other without

(Supplementary Fig. 1). Comparison of the structures of drSLC38A9 with and without an arginine at the TM1a site provides a possible model of arginine release and binding by drSLC38A9 in two different states (Fig. 3b). When open to the cytosol (state 1), TM1a is arrested by two polar interactions, Gln115-Thr391 and Asn116-Thr307, with TM5 and TM7, respectively. The TM1a anchor renders a new binding site next to TM1a for arginine, connecting the central binding site to the cytosol. The guanidinium group of arginine comes in proximity to the TM1a site and occupies this location between TM1a and TM8. When arginine is released (state 2), the TM1a binding site is emptied by solvent diffusion into the cytosolic vestibule. TM1a becomes unstable, and the TM1a anchor is broken from TM5 and TM7.

The anchoring system of TM1a, TM5 and TM7. In the present structure, anchoring of TM1a to TM5 and TM7 stabilizes drSLC38A9 in an intermediate state. The intricate interaction network between TM1a, TM5 and TM7 was found following binding of arginine (Fig. 3c). A salt bridge is formed between Asp116 and Thr307. While located next to Asp116, Trp115 is bonded to Thr391. Together, Trp115 and Asp116 mark the beginning of this anchor network on TM1a in the cytosol-open structure (Fig. 3c). The TM1a anchor suspends the helical segment of TM1a from its cytosolic end and contains a hydrophobic box formed by Met118 and Met119 sandwiched between Gln115 and Tyr392 (Fig. 3d). This hydrophobic box is immediately followed by the unwound region of TM1, suggesting that the TM1a anchor may cause Met119 to expose its carbonyl oxygen to disrupt the α-helix. Given the conservation of the WNTMM motif, a restrained TM1a in this conformation is likely to be important during transport by SLC38A9 homologs. Consistent with the structural insights mentioned above, an Asn128Ala substitution in the human homolog (hSLC38A9) has been shown to decrease transport activity[1]. While sequence alignment shows that
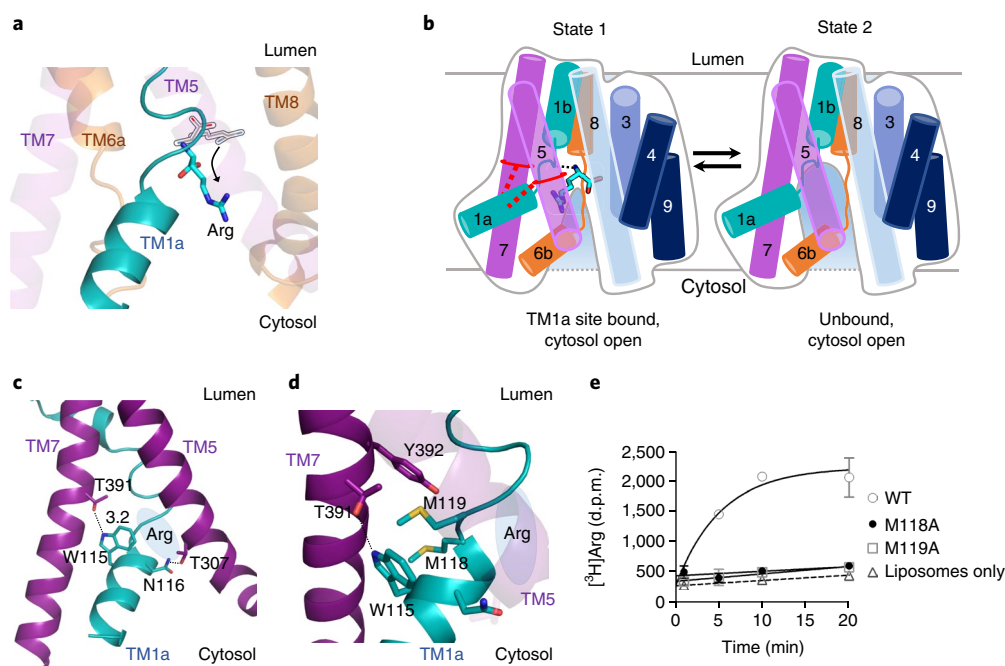
Fig. 3 | Arginine binding of drSLC38A9 stabilized by TM1a anchored by a hydrophobic box. a, Arginine bound by drSLC38A9 (blue stick) is pointing toward the cytosol, placing the guanidinium group between TM1a and TM8. A putative arginine (gray-lined hollow stick) at the central site is taken from AdiC (PDB 3L1L)[13] after structural alignment performed in PyMOL. AdiC to drSLC38A9; r.m.s. deviation = 3.57 Å, Cealign for 72 residues. The arrow shows the putative translocation of arginine during transport. **b**, Proposed cytosolic release of arginine by drSLC38A9. In state 1, arginine is bound at the TM1a binding site as elucidated in the crystal structure. TM1a is anchored by a pair of residues on TM5 and TM7, rendering a negatively charged binding site for arginine and connecting the central site to the cytosol. In state 2, arginine is released from the TM1a binding site. The TM1a anchor is weakened and cannot maintain interactions with TM5 and TM7. Two copies of drSLC38A9 are found in the asymmetric unit of the crystals, revealing arginine-bound and arginine-free cytosol-open states within the same crystal form. **c**, Polar interactions stabilize TM1a (cyan) between TM5 and TM7 (purple). Bonds of TM1a with TM5 and TM7 are shown as dashed lines. **d**, Hydrophobic box between TM1a and TM7. Met118 and Met119 are confined by Trp115 and Tyr392. **e**, Proteoliposome-based transport assay for arginine. Met118Ala and Met119Ala mutants show significant deficiency in arginine transport as compared to wild-type drSLC38A9. Error bars, represent s.e.m. from two independent proteoliposome preparations; n = 2 (Supplementary Dataset 2).

human Asn128 corresponds to Asn116 in the zebrafish homolog (Supplementary Note 1), disturbing Asn116 in the WNTMM motif on TM1a is believed to impair the anchoring network along with sodium coordination, which can consequently undermine transport. Met118Ala and Met119Ala substitutions in the WNTMM motif abolished transport of arginine, suggesting that the large, nonpolar side chains at this position are functionally important (Fig. 3e). Presumably, the two 'methionine fingers' insert into the hydrophobic box during conformational changes and draw TM1a to open at the cytosol. Tracing up from TM1a, TM1 and TM6 draw close at the GTS motif toward the luminal end. In the cytosol-open state of drSLC38A9, TM1a alone mediates arginine binding and forms a stabilized conformation. To achieve the same task, other LeuT-like transporters (for example, vSGLT and CaiT) use both TM1 and TM6 to retain substrates in the inward-open state, involving the GTS motif at disrupted regions[16,20].

Homology models of system A and system N transporters. This initial structural characterization of SLC38A9 allowed us to generate homology models for representatives of both system A (rat SLC38A2) and system N (rat SLC38A3) transporters (Fig. 4). These homology models appear to have many commonalities with the experimentally determined structure of drSLC38A9. A hydrophobic TM1a helix is present in both homology models, showing a preserved methionine-rich local structure. The experimentally verified sodium-binding site at Asn82 and Thr384 for rat SLC38A2 and Asn76 and Thr380 for rat SLC38A3 mutually supports the homology models[21–23]. The presence of tyrosine at residue 337 in rat

SLC38A2 and at residue 333 in rat SLC38A3 seems to be absolutely conserved in members of the SLC38 family, supporting the resembling hydrophobic center formed from TM1 and TM7 in the cytosol-open conformation. In TM3 of the homology models, both rat SLC38A2 and rat SLC38A3 contain a tyrosine side chain protruding into the cytosolic binding site, similarly to what we observed for Tyr204 in the drSLC38A9 structure (Supplementary Note 2), and hence TM3 likely also participates in substrate binding for rat SLC38A2 and rat SLC38A3. Interestingly, this tyrosine residue in TM3 is conserved in SNATs except for SNAT7 and SNAT8, in which the residue at this position is phenylalanine. From the two homology models in the cytosol-open conformation, we could not draw a clear distinction between system A and system N transporters. It is possible that the distinction would only manifest itself in other functional conformations of the transporters.

Discussion
In this work, we describe the first structure of drSLC38A9, captured in the cytosol-open state, and discover a new TM1a arginine-binding site in the transporter. The TM1a binding site consists of an anchor with two critical methionine fingers inserted into a hydrophobic box. Movement of the TM1a anchor is proposed to lead to an intermediate state during arginine uptake or release, which may regulate amino acid transport and modify the transport efficiency of the transporter in the presence of arginine. Notably, the intermediate state of SLC38A9 described in this study suggests that arginine binding could also affect the N terminus of the transporter by fixing TM1a, which directly links the transmembrane domain
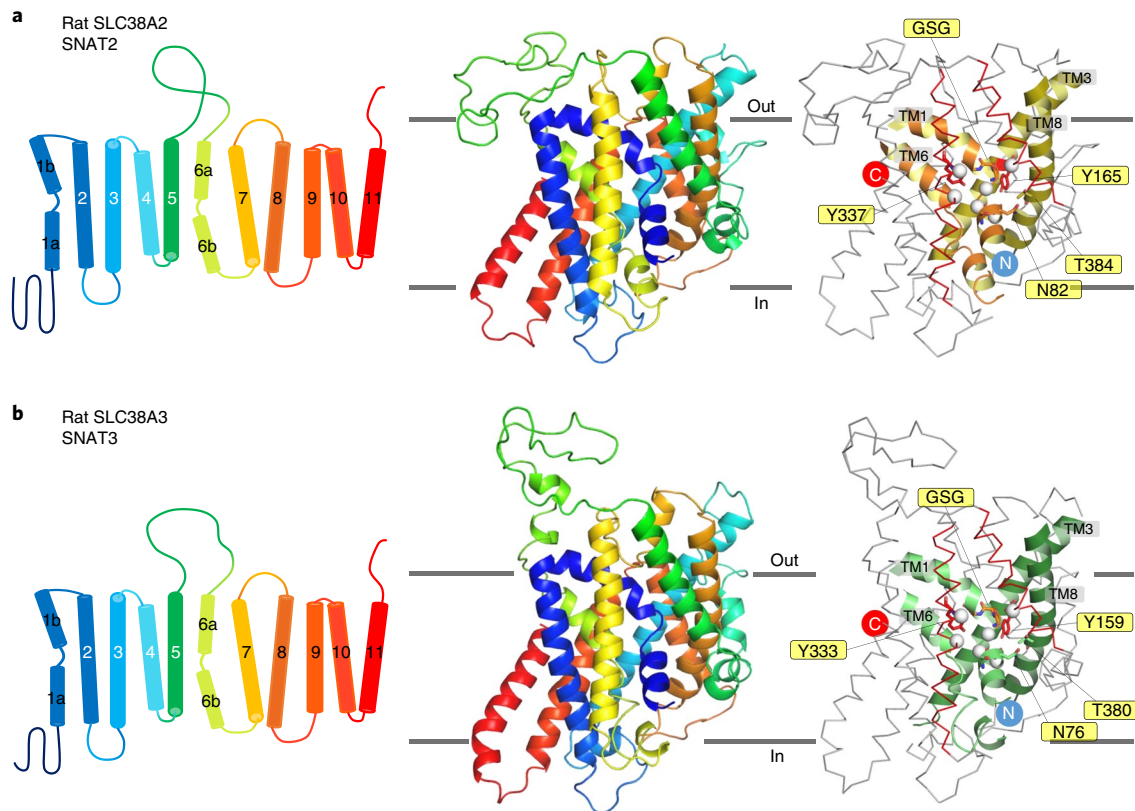
Fig. 4 | Comparative models of selected SNAT family members. a,b, Rat SLC38A2 (SNAT2) (**a**) and rat SLC38A3 (SNAT3) (**b**). Panels from left to right: topology, homology model and the hydrophobic box of the locally methionine-rich structure manifested in the homology models. Important residues are as indicated. Both homology models are depicted in the cytosol-open conformation. White spheres represent hydrophobic residues in the structures with the conserved tyrosine in TM7. Conserved residues within homologs of the proteins are labeled with text boxes. The orientation of the transporters in the membrane is indicated.

and the N-terminal domain of SLC38A9. However, structures of SLC38A9 with a visible N-terminal domain in different conformational states will be needed to elucidate the precise process by which this transporter binds to the Ragulator–Rag GTPase complex and to advance understanding on lysosomal amino acid transport and its modulation of the mTORC1 signaling pathway. While the sequence conservation between drSLC38A9 and the human protein is high[1,24] (Supplementary Note 1), we note that data on coupling drSLC38A9 to mTORC1 in zebrafish are limited and some differences between the human and zebrafish proteins may exist. Nonetheless, the structures presented here form the basis for future investigation into the function of these transceptors. Understanding of amino acid binding, transport and subsequent signaling by SLC38A9 could further assist the research community in combatting developmental and lysosomal-homeostasis-related disorders[25,26].

Methods

Methods, including statements of data availability and any associated accession codes and references, are available at https://doi.org/10.1038/s41594-018-0072-2.

References

1. Rebsamen, M. et al. SLC38A9 is a component of the lysosomal amino acid sensing machinery that controls mTORC1. *Nature* **519**, 477–481 (2015).
2. Wang, S. et al. Lysosomal amino acid transporter SLC38A9 signals arginine sufficiency to mTORC1. *Science* **347**, 188–194 (2015).
3. Jack, D. L., Paulsen, I. T. & Saier, M. H. The amino acid/polyamine/organocation (APC) superfamily of transporters specific for amino acids, polyamines and organocations. *Microbiology* **146**, 1797–1814 (2000).
4. Chang, H. C. & Bush, D. R. Topology of NAT2, a prototypical example of a new family of amino acid transporters. *J. Biol. Chem.* **272**, 30552–30557 (1997).
5. Saier, M. H. Jr et al. The Transporter Classification Database (TCDB): recent advances. *Nucleic Acids Res.* **44**(D1), D372–D379 (2016).
6. Västermark, Å. & Saier, M. H. Jr. Evolutionary relationship between 5 + 5 and 7 + 7 inverted repeat folds within the amino acid–polyamine–organocation superfamily. *Proteins* **82**, 336–346 (2014).
7. Shaffer, P. L., Goehring, A., Shankaranarayanan, A. & Gouaux, E. Structure and mechanism of a Na⁺-independent amino acid transporter. *Science* **325**, 1010–1014 (2009).
8. Wang, H. et al. Cloning and functional expression of ATA1, a subtype of amino acid transporter A, from human placenta. *Biochem. Biophys. Res. Commun.* **273**, 1175–1179 (2000).
9. Varoqui, H., Zhu, H., Yao, D., Ming, H. & Erickson, J. D. Cloning and functional identification of a neuronal glutamine transporter. *J. Biol. Chem.* **275**, 4049–4054 (2000).
10. Bröer, S. The SLC38 family of sodium–amino acid co-transporters. *Pflugers Arch.* **466**, 155–172 (2014).
11. Christensen, H. N. Role of amino acid transport and countertransport in nutrition and metabolism. *Physiol. Rev.* **70**, 43–77 (1990).
12. Schiöth, H. B., Roshanbin, S., Hägglund, M. G. A. & Fredriksson, R. Evolutionary origin of amino acid transporter families SLC32, SLC36 and SLC38 and physiological, pathological and therapeutic aspects. *Mol. Aspects Med.* **34**, 571–585 (2013).
13. Gao, X. et al. Mechanism of substrate recognition and transport by an amino acid antiporter. *Nature* **463**, 828–832 (2010).
14. Krishnamurthy, H. & Gouaux, E. X-ray structures of LeuT in substrate-free outward-open and apo inward-open states. *Nature* **481**, 469–474 (2012).

15. Ressl, S., Terwisscha van Scheltinga, A. C., Vonrhein, C., Ott, V. & Ziegler, C. Molecular basis of transport and regulation in the Na$^+$/betaine symporter BetP. *Nature* **458**, 47–52 (2009).
16. Schulze, S., Köster, S., Geldmacher, U., Terwisscha van Scheltinga, A. C. & Kühlbrandt, W. Structural basis of Na$^+$-independent and cooperative substrate/product antiport in CaiT. *Nature* **467**, 233–236 (2010).
17. Malinauskaite, L. et al. A mechanism for intracellular release of Na$^+$ by neurotransmitter/sodium symporters. *Nat. Struct. Mol. Biol.* **21**, 1006–1012 (2014).
18. Wyant, G. A. et al. mTORC1 activator SLC38A9 is required to efflux essential amino acids from lysosomes and use protein as a nutrient. *Cell* **171**, 642–654 (2017).
19. Watanabe, A. et al. The mechanism of sodium and substrate release from the binding pocket of vSGLT. *Nature* **468**, 988–991 (2010).
20. Faham, S. et al. The crystal structure of a sodium galactose transporter reveals mechanistic insights into Na$^+$/sugar symport. *Science* **321**, 810–814 (2008).
21. Zhang, Z., Gameiro, A. & Grewer, C. Highly conserved asparagine 82 controls the interaction of Na$^+$ with the sodium-coupled neutral amino acid transporter SNAT2. *J. Biol. Chem.* **283**, 12284–12292 (2008).
22. Zhang, Z., Albers, T., Fiumera, H. L., Gameiro, A. & Grewer, C. A conserved Na$^+$ binding site of the sodium-coupled neutral amino acid transporter 2 (SNAT2). *J. Biol. Chem.* **284**, 25314–25323 (2009).
23. Bröer, S., Schneider, H. P., Bröer, A. & Deitmer, J. W. Mutation of asparagine 76 in the center of glutamine transporter SNAT3 modulates substrate-induced conductances and Na$^+$ binding. *J. Biol. Chem.* **284**, 25823–25831 (2009).
24. Castellano, B. M. et al. Lysosomal cholesterol activates mTORC1 via an SLC38A9–Niemann-Pick C1 signaling complex. *Science* **1311**, 1306–1311 (2017).
25. Efeyan, A., Zoncu, R. & Sabatini, D. M. Amino acids and mTORC1: from lysosomes to disease. *Trends Mol. Med.* **18**, 524–533 (2012).
26. Platt, F. M. Emptying the stores: lysosomal diseases and therapeutic strategies. *Nat. Rev. Drug Discov.* **17**, 133–150 (2018).

Author contributions
H.-T.L., J.M. and T.G. designed the project. H.-T.L. and J.M. performed experiments, including protein preparation, antibody screening, crystallization and data collection. H.-T.L. performed model building and refinement. S.S.M. and H.-T.L. performed the radioligand uptake assay. H.-T.L., J.M. and T.G. participated in data analysis and figure preparation. H.-T.L., J.M. and T.G. wrote the manuscript.

Competing interests
The authors declare no competing interests.

Additional information
Supplementary information is available for this paper at https://doi.org/10.1038/s41594-018-0072-2.

Reprints and permissions information is available at www.nature.com/reprints.

Correspondence and requests for materials should be addressed to T.G.

Publisher's note: Springer Nature remains neutral with regard to jurisdictional claims in published maps and institutional affiliations.

Methods

drSLC38A9 cloning, expression and purification. The sequence encoding N-terminally truncated drSLC38A9 (GenBank Q08BA4), ΔN-SLC38A9, was cloned into the pFastBac-1 vector (Invitrogen) with a sequence encoding an N-terminal 8×His tag and a thrombin cleavage site. Four mutations (encoding Asn227Gln, Asn235Gln, Asn252Gln and Asn263Gln) were introduced at the glycosylation sites. Plasmids were transformed into DH10bac for preparation of bacmids. Recombinant baculovirus was generated and used for transfection following the protocol provided for the Bac-to-bac Baculovirus Expression System. ΔN-SLC38A9 was overexpressed in *Spodoptera frugiperda* Sf-9 insect cells, which were harvested 60 h after infection. Cell pellets were resuspended in lysis buffer containing 20 mM Tris (pH 8.0) and 150 mM NaCl and supplemented with protease inhibitor cocktail (Roche). Forty homogenizing cycles were then carried out to break cells on ice, followed by centrifugation at 130,000 g for 1 h. Pelleted membrane was resuspended and washed in high-salt buffer containing 1.6 M NaCl and 20 mM Tris (pH 8.0) and centrifuged again for 1 h at 130,000 g. The pelleted membrane was frozen in liquid nitrogen and stored at –80 °C until further use. To purify ΔN-SLC38A9, the membrane pellet was solubilized in 2% *n*-dodecyl-β-ᴅ-maltopyranoside (DDM), 20 mM Tris (pH 8.0), 150 mM NaCl, 5% glycerol and 0.2% cholesteryl hemisuccinate Tris salt (CHS) for 4 h at 4 °C, followed by centrifugation for 1 h at 130,000 g. 20 mM imidazole (pH 8.2) was added to the supernatant before incubation with TALON beads for 16 h at 4 °C. ΔN-SLC38A9-bound beads were washed with 6 column volumes of 20 mM imidazole, 20 mM Tris (pH 8.0), 500 mM NaCl and 0.1% DDM. The resins were then equilibrated in buffer composed of 20 mM Tris (pH 8.0), 150 mM NaCl, 0.4% decyl-β-ᴅ-maltoside (DM) and 0.02% DDM. At 4 °C, the 8×His tag was removed by on-column thrombin digestion overnight at an enzyme:protein molar ratio of 1:500. The cleaved ΔN-SLC38A9 was collected in flow-through and was flash frozen in liquid nitrogen and stored at –80 °C until use. Se-Met-substituted ΔN-SLC38A9 was overexpressed in Sf-9 cells using the same procedures described above for native protein except that 100 mg/L seleno-methionine (Acros Organics) was added to cultures during the course of the 60-h period following infection. The purification procedure for Se-Met-substituted ΔN-SLC38A9 was the same as for the native protein.

Fab production and purification. Mouse IgG monoclonal antibodies against ΔN-SLC38A9 were produced by the Monoclonal Antibody Core (D. Cawley). 330 μg of purified ΔN-SLC38A9 in buffer containing 20 mM Tris (pH 8.0), 150 mM NaCl, 0.02% DDM and 0.002% CHS was used to immunize mice in three injections. 15×96-well plate fusions yielded 169 IgG-positive wells at a 1:30 dilution. Native and denatured ΔN-SLC38A9 proteins were then used in ELISA to search for candidates that bound the conformational epitopes[27], where Ni-NTA plates were used for ΔN-SLC38A9 immobilization. Thirty-five of the 169 fusions showed significant preference for binding against well-folded ΔN-SLC38A9. Western blotting was performed to assess the binding affinity and specificity of the antibodies generated from hybridoma cell lines. Monoclonal antibody 11D3 was then purified from the hybridoma supernatants by 4-mercaptoethylpyridine (MEP) chromatography. Fab fragments were produced by papain digestion and purified in flow-through buffer containing 20 mM NaPi (pH 8.0) and 150 mM NaCl by protein A affinity chromatography.

Assembly of ΔN-SLC38A9–Fab complex. Purified Fab fragment of 11D3 was added to ΔN-SLC38A9 at a 2:1 molar ratio, and the components were incubated for 4 h to form stable complexes. ΔN-SLC38A9–11D3 was concentrated by centrifugal filter vivaspin 20 at 50 kDa MWCO. The concentrated protein was further purified and underwent detergent exchange by gel filtration, Superdex-200 size-exclusion column, in buffer containing 20 mM Tris (pH 8.0), 150 mM NaCl and 0.2% DM. As judged by SDS–PAGE and size-exclusion chromatography elution profile (Supplementary Fig. 4), fractions containing appropriate ΔN-SLC38A9–11D3 complexes were pooled and concentrated to 5 mg/ml for crystallization.

Crystallization. An initial hanging-drop crystallization assay with purified ΔN-SLC38A9 produced crystals grown under the condition of 30% PEG400, 100 mM Tris (pH 8.0) and 400 mM LiCl at 4 °C. However, these crystals gave anisotropic diffraction to around 6 Å. Crystals showing adequate diffraction power were obtained only when ΔN-SLC38A9 was co-crystallized as a complex with Fab prepared from hybridoma cell line 11D3 (IgG2a, kappa). The best crystal, which diffracted to 3.1 Å, was obtained under the condition of 26–30% PEG400, 100 mM ADA (pH 7.2) and 350 mM Li₂SO₄ at 4 °C. Before data collection, the crystals were soaked in the same crystallizing solution containing 30% PEG400 and 20 mM arginine (pH 7.2) for 1 h, and were rapidly frozen in liquid nitrogen. Se-Met crystals were grown and harvested in the same manner as the native crystals.

Data collection and structure refinement. X-ray diffraction datasets were collected at the Advanced Photon Source (Argonne National Laboratory, beamlines 24-IDC and 24-IDE) and processed in the online server RAPD, which uses XDS and the CCP4 suite package for integrating and scaling to resolutions of 3.1 Å (native) and 3.4 Å (Se-Met). Antigen-binding fragments (Fab) from PDB 1F8T[28] were used in the initial molecular replacement as the search model. The Se-Met dataset was then phased by single anomalous dispersion in Phenix[29]

using differences from 23 selenium atoms at λ = 0.9791 Å and the two Fab fragments previously placed using Phaser as a partial model (MRSAD)[28]. Helices were manually placed in the density-modified map and extended using Coot[30]. Subsequent cycles of density modification, model building and refinement were carried out in Phenix and Coot until structure completion. The final model contains two molecules of ΔN-SLC38A9 (residues 108–549) and two pairs of the heavy-light chain of Fab in an asymmetric unit. Data collection and refinement statistics are presented in Table 1.

Preparation of proteoliposomes. Full-length and N-terminally truncated drSLC38A9 proteins were expressed and purified as described above. Liposomes were prepared by resuspending thin films of 35 mg/ml egg phosphatidylcholine (egg-PC) in buffer A (20 mM MES pH 5.0 and 1 mM DTT, with various concentrations of NaCl), followed by extrusion through membranes with a pore size of 0.4 μm. Triton X-100 was added to the extruded liposomes at a 10:1 (wt/wt) lipid:detergent ratio. The volume was then adjusted to a final concentration of 14 mg egg-PC/ml with buffer A and incubated for 1 h, followed by reconstituting drSLC38A9 or ΔN-SLC38A9 at a protein:lipid ratio of 1:400 (wt/wt) for 2 h. Detergents using removed by SM2 Bio-Beads (Bio-Rad) added to the protein–lipid mix and rotated overnight at 4 °C. The next day, proteoliposomes were collected, aliquotted and stored at –80 °C. For the KCl and NMG assay groups, the wild-type drSLC38A9 protein was reconstituted to the liposomes in the presence of buffer B (20 mM potassium succinate pH 5.0 and 100 mM KCl) or buffer C (20 mM NMG succinate pH 5.0 and 100 mM NMG HCl). To fully incorporate the buffer, the liposomes were pelleted by ultracentrifugation and resuspended in buffer B or buffer C before the reactions.

Radioligand uptake assays. Proteoliposomes of reconstituted drSLC38A9, ΔN-SLC38A9, Met118Ala and Met119Ala mutants were thawed on ice. For transport assays of various constructs, transport reactions were initiated by adding [³H]ʟ-arginine (American Radiolabeled Chemicals) to 100-μl aliquots of proteoliposomes containing 24 pmol of protein to a final concentration of 0.5 μM [³H]ʟ-arginine. For transport assays in the presence of various cations, the pelleted liposomes were resuspended in buffer B or C, before being added to the respective buffer supplemented with 0.5 μM [³H]ʟ-arginine at the dilution of 1:20 volume ratio. A negative control with protein-free liposomes was carried out in parallel to the experiment groups. At various time points, proteoliposomes were filtered, washed with 10 ml of buffer and collected on 0.22-μm GSWP nitrocellulose membranes. 10 ml of scintillation fluid was then added to each filter in a vial and counted. A time-course profile indicates that the retained radioligands reached saturation in 10 min. Measurements at various time points of arginine uptake were plotted to establish the transport comparisons between various constructs of drSLC38A9. Each of the experiments was repeated two or three times.

Reporting Summary. Further information on experimental design is available in the Nature Research Reporting Summary linked to this article.

Comparative modeling. From the crystal structure of drSLC38A9–11D3 (PDB accession number: 6C08), the coordinates of drSLC38A9 were extracted and used as a template input in SWISS-MODEL for modeling under automated mode[31].

Data availability. The atomic coordinates and structure factors of drSLC38A9–Fab have been deposited in PDB under accession 6C08. Source data for Figs. 1c,d and 3e are available with the paper online. Other data are available from the corresponding author upon reasonable request.

All figures in this paper were prepared with PyMOL v1.8.6.0[32] and assembled in Microsoft PowerPoint v15.18. Supplementary Note 1 was prepared using the program Clustal Omega[33] for alignments and ESPript 3.0[34] for styling.

References

27. Lim, H. H., Fang, Y. & Williams, C. High-efficiency screening of monoclonal antibodies for membrane protein crystallography. *PLoS One* **6**, e24653 (2011).
28. Fokin, A. V. et al. Spatial structure of a Fab-fragment of a monoclonal antibody to human interleukin-2 in two crystalline forms at a resolution of 2.2 and 2.9 angstroms. *Bioorg. Khim.* **26**, 571–578 (2000).
29. Adams, P. D. et al. PHENIX: a comprehensive Python-based system for macromolecular structure solution. *Acta Crystallogr. D Biol. Crystallogr.* **66**, 213–221 (2010).
30. Emsley, P., Lohkamp, B., Scott, W. G. & Cowtan, K. Features and development of Coot. *Acta Crystallogr. D Biol. Crystallogr.* **66**, 486–501 (2010).
31. Biasini, M. et al. SWISS-MODEL: modelling protein tertiary and quaternary structure using evolutionary information. *Nucleic Acids Res.* **42**, W252–W258 (2014).
32. Schrödinger, L. The PyMOL Molecular Graphics System, Version 2.0 (Schrödinger, LLC, 2015).
33. Sievers, F. et al. Fast, scalable generation of high-quality protein multiple sequence alignments using Clustal Omega. *Mol. Syst. Biol.* **7**, 539 (2011).
34. Robert, X. & Gouet, P. Deciphering key features in protein structures with the new ENDscript server. *Nucleic Acids Res.* **42**, W320–W324 (2014).

naturereseach

Corresponding author(s):   Tamir Gonen

Reporting Summary

Nature Research wishes to improve the reproducibility of the work that we publish. This form provides structure for consistency and transparency in reporting. For further information on Nature Research policies, see Authors & Referees and the Editorial Policy Checklist.

Statistical parameters

When statistical analyses are reported, confirm that the following items are present in the relevant location (e.g. figure legend, table legend, main text, or Methods section).

n/a	Confirmed	
☐	☒	The exact sample size (n) for each experimental group/condition, given as a discrete number and unit of measurement
☐	☒	An indication of whether measurements were taken from distinct samples or whether the same sample was measured repeatedly
☐	☒	The statistical test(s) used AND whether they are one- or two-sided *Only common tests should be described solely by name; describe more complex techniques in the Methods section.*
☐	☒	A description of all covariates tested
☒	☐	A description of any assumptions or corrections, such as tests of normality and adjustment for multiple comparisons
☐	☒	A full description of the statistics including central tendency (e.g. means) or other basic estimates (e.g. regression coefficient) AND variation (e.g. standard deviation) or associated estimates of uncertainty (e.g. confidence intervals)
☐	☒	For null hypothesis testing, the test statistic (e.g. F, t, r) with confidence intervals, effect sizes, degrees of freedom and P value noted *Give P values as exact values whenever suitable.*
☒	☐	For Bayesian analysis, information on the choice of priors and Markov chain Monte Carlo settings
☒	☐	For hierarchical and complex designs, identification of the appropriate level for tests and full reporting of outcomes
☒	☐	Estimates of effect sizes (e.g. Cohen's d, Pearson's r), indicating how they were calculated
☐	☒	Clearly defined error bars *State explicitly what error bars represent (e.g. SD, SE, CI)*

Our web collection on statistics for biologists may be useful.

Software and code

Policy information about availability of computer code

Data collection	NECAT APS 24ID-C
Data analysis	PHENIX, Coot, PyMOL and other software listed in the Method section.

For manuscripts utilizing custom algorithms or software that are central to the research but not yet described in published literature, software must be made available to editors/reviewers upon request. We strongly encourage code deposition in a community repository (e.g. GitHub). See the Nature Research guidelines for submitting code & software for further information.

Data

Policy information about availability of data

All manuscripts must include a data availability statement. This statement should provide the following information, where applicable:
- Accession codes, unique identifiers, or web links for publicly available datasets
- A list of figures that have associated raw data
- A description of any restrictions on data availability

The atomic coordinates and the structure factors of drSLC38A9-Fab have been deposited in the PDB under accession code 6C08. Source data for figure 1c, 1d and 3e are available with the paper online. Other data were available from the corresponding author upon reasonable requests.

Field-specific reporting

Please select the best fit for your research. If you are not sure, read the appropriate sections before making your selection.

☒ Life sciences   ☐ Behavioural & social sciences   ☐ Ecological, evolutionary & environmental sciences

For a reference copy of the document with all sections, see nature.com/authors/policies/ReportingSummary-flat.pdf

Life sciences study design

All studies must disclose on these points even when the disclosure is negative.

Sample size	present in relevant figure legends
Data exclusions	no data exclusions
Replication	present in relevant figure legends
Randomization	no randomization
Blinding	no blinding

Reporting for specific materials, systems and methods

Materials & experimental systems

n/a	Involved in the study
☒	☐ Unique biological materials
☐	☒ Antibodies
☐	☒ Eukaryotic cell lines
☒	☐ Palaeontology
☒	☐ Animals and other organisms
☒	☐ Human research participants

Methods

n/a	Involved in the study
☒	☐ ChIP-seq
☒	☐ Flow cytometry
☒	☐ MRI-based neuroimaging

Antibodies

Antibodies used	Antibody 11D3 was developed and mixed with SLC38A9 for crystallization
Validation	structure validation report

Eukaryotic cell lines

Policy information about cell lines

Cell line source(s)	Spodoptera frugiperda Sf9 cell line from Expression Systems, LLC
Authentication	N/A
Mycoplasma contamination	N/A
Commonly misidentified lines (See ICLAC register)	N/A